

## Spatiotemporal scaling properties of the ground geomagnetic field variations

Antti Pulkkinen,<sup>1</sup> Alex Klimas,<sup>1</sup> Dimitris Vassiliadis,<sup>1</sup> Vadim Uritsky,<sup>2</sup> and Eija Tanskanen<sup>3</sup>

Received 30 June 2005; revised 25 November 2005; accepted 30 November 2005; published 17 March 2006.

[1] The spatiotemporal scaling properties of the auroral region ground horizontal magnetic field fluctuations are investigated in terms of structure function analysis. First, the distorting effects of the continuation of the magnetic field from the ionosphere to the ground level and the effects of the geomagnetic induction on the derived scalings are studied. It is found that the spatial fluctuations of the magnetic field and its time derivative are distorted by the field continuation in the ranges of scales of the data, i.e.,  $100 < \Delta r < 2400$  km (above  $\sim 1000$  km, analysis is spatially one-dimensional) and  $10 < \tau < 10^4$  s. Specifically, the extent of the distortion is found to be dependent on the original ionospheric level scaling of the fluctuations. The effect of the geomagnetic induction is found to be negligible in the ranges of scales of the data. The main findings of the study are (1) there is a significant change in the dynamics of the field fluctuations in the range  $80 < \tau < 100$  s where the time derivative of the magnetic field undergoes a transition from correlated to uncorrelated temporal behavior, (2) the spatiotemporal behavior of the time derivative of the magnetic field above temporal scales of 100 s resembles that of uncorrelated white noise, (3) the spatial symmetry of the field fluctuations increases during substorms, indicating the presence of spatially less ordered ionospheric equivalent currents, and (4) the spatial scaling properties of the field fluctuations may explain why the magnetotelluric sounding method works better than expected in auroral regions.

**Citation:** Pulkkinen, A., A. Klimas, D. Vassiliadis, V. Uritsky, and E. Tanskanen (2006), Spatiotemporal scaling properties of the ground geomagnetic field variations, *J. Geophys. Res.*, *111*, A03305, doi:10.1029/2005JA011294.

### 1. Introduction

[2] Observations both on the ground and in space have revealed the spatiotemporally highly variable nature of the solar wind-magnetosphere-ionosphere system: physical parameters vary in a complex manner over wide ranges of scales both in time and space. The variability underscores the need for a proper statistical description of the observations since attempts to explain individual observations may be doomed by the complex dynamics of the system. In an ideal case, a successful statistical description accurately characterizing the data can enable identification of the underlying dynamics by connecting the observed statistics to the statistics of a model enlightening the fundamentals of the phenomenon, for example, by explaining how the complexity arises. Such models, having varying degrees of mathematical rigor, include a wide selection of random

processes, turbulence and self-organized criticality (SOC). Of these especially SOC has been recently drawing wide interest in explaining complex spatiotemporal structures in natural dynamical systems, such as space plasmas [see, e.g., Watkins *et al.*, 2001; Hergarten, 2002; Klimas *et al.*, 2004; Chang and Tam, 2004].

[3] A great number of earlier investigations have addressed the observed statistics and their relation to underlying dynamics of the solar wind [e.g., Burlaga, 1995, and references therein], magnetosphere [e.g., Borovsky, 2004, and references therein], and ionosphere [e.g., Buchert *et al.*, 1999; Abel and Freeman, 2002]. A large number of similarly oriented investigations have studied the statistical behavior of the ground magnetic field variations, most of these studies focusing on the analysis of geomagnetic indices like *AL*, *AU*, *AE* [e.g., Hnat *et al.*, 2002; Consolini and De Michelis, 2005] or *D<sub>st</sub>* [Wanliss, 2005]. Despite the large number of investigations, no coherent picture of the near-Earth space dynamics has emerged yet. Different analysis techniques applied to different data sets and limited ranges of scales over which, for example, power law behavior of the data are found create ambiguity that complicate further interpretations. One of the largest shortcomings in the studies of the near space dynamics is that we rely essentially on point measurements in a vast space.

<sup>1</sup>NASA Goddard Space Flight Center, Greenbelt, Maryland, USA.

<sup>2</sup>Institute of Physics and Physics Department, St. Petersburg State University, St. Petersburg, Russia.

<sup>3</sup>Space Research Unit, Finnish Meteorological Institute, Helsinki, Finland.

Thus, though some suggestions also about spatial behavior can be made, for example, by assuming static moving structures, basically only temporal analysis can be carried out. This severely limits the capability to identify the origin of the observed dynamics.

[4] At the moment, the only means to carry out comprehensive spatiotemporal analysis of the near-Earth space-related data is to use remote sensing measurements of ionospheric dynamics, i.e., ionospheric radar, auroral emission, ground based magnetometer network or similar data. Examples of such work are recent spatiotemporal analyses of space-based and ground-based images of auroral emissions carried out to investigate the ionospheric dynamics in the SOC context [Lui *et al.*, 2000; Uritsky *et al.*, 2002; Kozelov *et al.*, 2004]. We also note that there are ongoing activities to carry out spatiotemporal analysis of the ionospheric drift velocities using coherent scatter radar data [Abel *et al.*, 2004]. However, thus far, no spatiotemporal analysis of the ground magnetometer data exists.

[5] Accordingly, the goal of the work at hand is to statistically characterize the spatiotemporal fluctuations of the ground magnetic field in the auroral region. To reach this goal, we will use data from the IMAGE magnetometer array (<http://www.ava.fmi.fi/image>) that enable analysis of long time series (10 s resolution starting from 1993) and spatial scales ranging from about 100 km up to about 2400 km.

[6] We will show that, despite the distortions characteristic for ground magnetic field data, spatiotemporal characterization of the external magnetic field fluctuations, i.e., ionospheric equivalent current fluctuations can be derived by applying the techniques used here. We will also show that the derived statistics can give us important insights into the nature of these fluctuations having implications regarding the solar wind-magnetosphere driver. As an addition to space-oriented focus, we will demonstrate that understanding the statistical characteristics of the ground magnetic field variations can also help to understand why the magnetotelluric sounding method [Cagniard, 1953] used in solid Earth studies works also in the auroral region. The magnetotelluric sounding method is used to map the spatial variation of the Earth's resistivity by measuring naturally occurring electric and magnetic fields at the Earth's surface (for more details on the method, see, for example, *Berdichevsky and Zhdanov* [1984]).

[7] It is emphasized at this point that only ground magnetic field recordings are used in the analysis carried out here. It follows, that the results can be interpreted only in terms of ionospheric equivalent, not in terms of true ionospheric currents [see, e.g., *Untiedt and Baumjohann*, 1993]. However, equivalent currents still can shed light on spatial and temporal scales of the basic processes in the ionosphere. In addition, ground magnetic field data needed for the derivation of equivalent currents are easily available in dense networks, which is not true for radar and satellite data that are needed for the full solution of the ionospheric electrodynamic.

[8] The structure of the work is as follows. First, in section 2.1, we briefly review the statistical analysis method used in the investigation and a detailed description of the application of the method to IMAGE magnetometer array data is given. There are some important issues peculiar to

the statistical analysis of ground magnetometer recordings. These issues will be addressed in sections 2.2 and 2.3 where we will look closely at how the magnetic field continuation and the geomagnetic induction may distort the scaling results obtained here. Then in section 3, the results of the IMAGE data analysis are shown and the main features of the results are described. In section 4 we investigate how the findings of section 3 may bring new understanding into solid Earth studies using geoelectromagnetic sounding methods. Finally, in sections 5 and 6, we discuss the implications of the results and give a brief summary of the work, respectively.

## 2. Statistical Analysis

[9] From a myriad of different statistical analysis methods it is usually all but obvious which method should be applied to the data to be investigated. Optimally, a number of different methods should be applied and the results compared. We select the structure function analysis method based on the following criteria: (1) it is very straightforward to apply in a spatiotemporal sense, and (2) the method is applied widely, for example, in the analysis of turbulence [e.g., *Bohr et al.*, 1998] and in the analysis of surface growth processes [e.g., *Barabási and Stanley*, 1995], thus providing a collection of models to which the observed statistics can be compared. In addition, the structure function has some pleasant mathematical properties that enable tractable theoretical considerations, as will be seen below.

[10] Before going to the analysis of the actual data, we need to consider some issues peculiar to the statistical analysis of ground magnetometer recordings. First, depending on the position of the auroral oval, magnetometers "scan" fluctuations in polar cap, auroral oval and subauroral current systems which may all have their distinct statistical features. Thus it may be difficult to interpret which features in the derived overall statistics reflect the characteristics of each of those regions. However, due to the already limited spatial range (just one order of magnitude) of the IMAGE array (Figure 1), we do not want to limit here our data by focusing only, for example, on the region right below the maximum of the current amplitude, i.e., on the auroral oval region. Also, due to the fact that the largest distances in the IMAGE array are in the north-south direction, it is possible that for large spatial separations (above  $\sim 1000$  km) the derived structure functions have bias to differences in the north-south direction. This in effect means that at large spatial scales the analysis is essentially spatially one-dimensional. In addition to ambiguities caused by the spatial structure of the magnetometer array, assuming that the majority of the signal originates from the ionosphere, the fact that the source for the magnetic field variations is located about 100 km above the plane of measurements causes spatial distortions of the original statistical scaling of the source currents. This problem refers to the so-called continuation of the magnetic field through a source-free region [see, e.g., *Amm and Viljanen*, 1999]. Finally, geomagnetic induction in the Earth produces an additional component of internal origin to the derived statistics and may mask the source characteristics that are of our main interest. Accordingly, one not only needs to be careful in selecting the appropriate tools for the analysis but

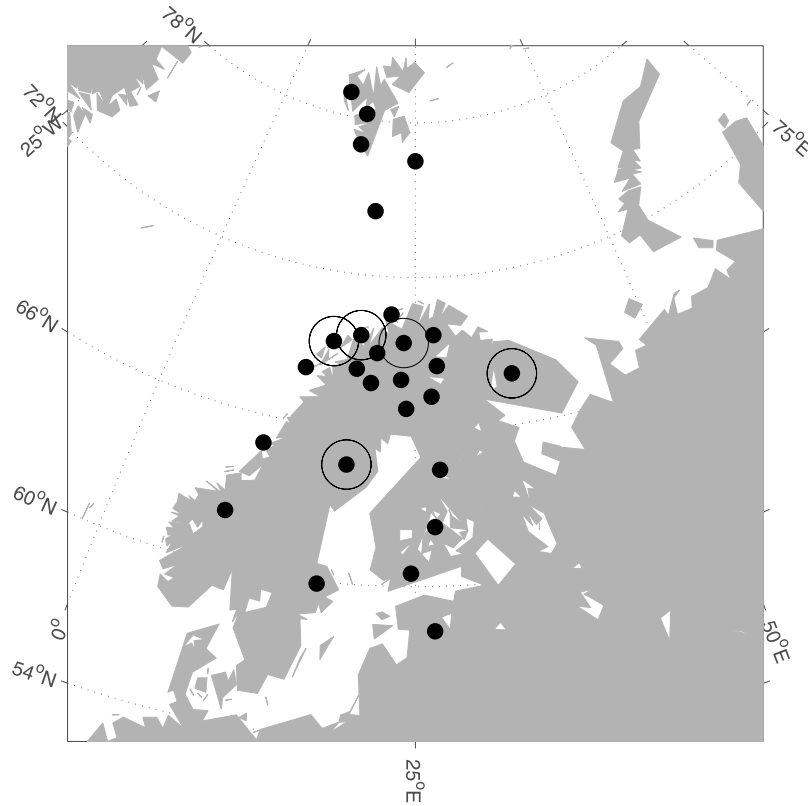


**Figure 1.** IMAGE magnetometer array. Circles show the stations excluded from the statistical analysis. Geographic coordinates are used.

also in understanding how different distortions affect the derived statistics. These distorting effects will be investigated in detail below.

[11] We note that the effects of the magnetic field continuation and the geomagnetic induction could be eliminated in theory by first carrying out the separation of the ground magnetic field into external and internal parts [see *Pulkkinen et al., 2003*, and references therein] and by then carrying out the magnetic field continuation of the external part to the ionospheric level. However, additional modeling of the data would inevitably introduce artificial cutoffs to the computed structure functions and thus only raw magnetic data is analyzed here.

## 2.1. Structure Function Analysis

[12] Spatiotemporal structure function analysis of variable  $a$  is carried out by using the following expression:

$$S^2(\Delta\mathbf{r}, \tau) = \langle |a(t, \mathbf{r}) - a(t + \tau, \mathbf{r} + \Delta\mathbf{r})|^2 \rangle \quad (1)$$

where  $\langle \cdot \rangle$  denotes the expectation value. Ideally, for example in multifractal analysis [see, e.g., *Burlaga, 1995*], also higher moments (i.e., larger exponents than 2) of the structure function are applied. However, to keep the interpretation of our results tractable we will focus here only on the second moment. Note below, that although we actually compute the second moment  $S^2(\Delta\mathbf{r}, \tau)$ , all the plots are given as  $S(\Delta\mathbf{r}, \tau)$ , i.e., as a square root of the original function.

[13] Let us then briefly review a few basic properties of the structure function. For simplicity, we omit the  $\Delta\mathbf{r}$  dependence and write the expectation value explicitly as

$$S^2(\tau) = \langle |\Delta a(\tau)|^2 \rangle = \int_{-\infty}^{\infty} P(\Delta a) |\Delta a|^2 d(\Delta a) \quad (2)$$

where  $P$  denotes the probability density function. By definition, for a self-affine stochastic variable  $\Delta a$  it holds that [see, e.g., *Hergarten, 2002*, p. 53]

$$P(\Delta a) = \tau^{-H} P_s(\Delta a \tau^{-H}) \quad (3)$$

where  $s$  denotes the rescaled probability density function. Then, we obtain from equation (2) by carrying out substitution  $\Delta a' = \Delta a \tau^{-H}$

$$S^2(\tau) = \tau^{2H} \int_{-\infty}^{\infty} P_s(\Delta a') |\Delta a'|^2 d(\Delta a') \sim \tau^{2H} \quad (4)$$

It is thus clear that the scaling of the structure function as defined by equation (1) is via Relation (3) in a close relationship with the temporal scaling of the probability density function of fluctuations  $\Delta a$ . For white noise, the structure function scales trivially in time as  $S^2(\tau) \sim c$ ,  $c$  being a constant. For diffusive processes, like Brownian motion, the scaling obeys  $S^2(\tau) \sim \tau$ . Generally, for fractional Brownian motion (having white noise and Brownian motion as its subclasses) the scaling obeys

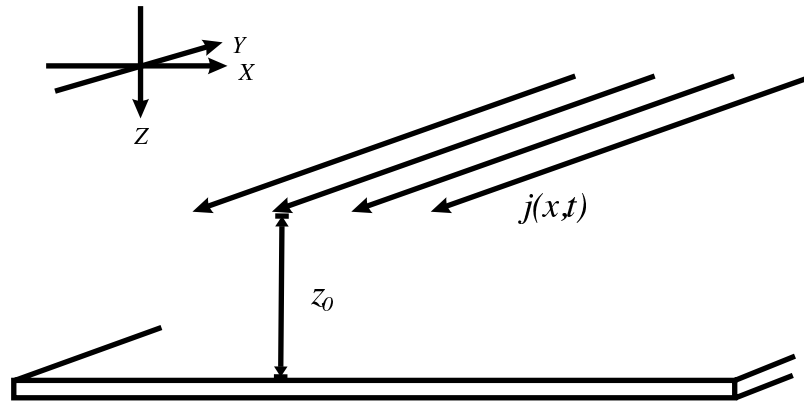


**Figure 2.** Image of setting used to investigate the effects of the magnetic field continuation. One-dimensional current layer  $j(x, t)$  flowing along the  $y$  axis at height  $z_0$  above the ground. The surface of the Earth is at the origin of the  $z$  axis.

$S^2(\tau) \sim \tau^{2H}$ . Note that all of these properties are based on the self-affinity of the process, i.e., the statistical properties of the phenomenon are not changed under scale transformation.

[14] Here the structure function is computed as a function of radial distance  $\Delta r$  along the surface of the Earth and time lag  $\tau$  for variables  $B_x, B_y, dB_x/dt$  and  $dB_y/dt$  where  $B$  denotes the ground magnetic field and  $x$  and  $y$  denote the geomagnetic north and east components, respectively. The first two variables reflect the spatiotemporal variations of the ionospheric equivalent currents [see, e.g., *Untiedt and Baumjohann, 1993*], the third and fourth variables of interest are in turn related to the geoelectric field induced at the surface of Earth [e.g., *Viljanen et al., 2001*]. Statistical characteristics of the geoelectric field have importance, for example, for studies of the ground effects of space weather [see, e.g., *Pulkkinen, 2003*, and references therein]. We first map the  $(nm)^2$  data points, where  $n$  is the number of stations and  $m$  the number of temporal steps, to  $(\Delta r, \tau)$  space which is then divided into logarithmic bins. For each bin we select  $N$  points from the  $(\Delta r, \tau)$  space, evaluate  $S^2(\Delta r, \tau)$  and then compute the average. The points are selected so that each bin contains an equal number of both spatial and temporal pairs. 10 spatial pairs and 10,000 points in general for each bin were selected for one day of 10 s IMAGE array data. Computed averages were assigned to the value in the middle of the bin boundaries.

## 2.2. Effects of the Magnetic Field Continuation

[15] Let us then investigate the effect of the magnetic field continuation. We will assume planar geometry which is reasonable for local investigations like the one carried out here [see, e.g., *Viljanen et al., 2004*]. Imagine the following simplified situation: we have an infinitely thin one-dimensional ionospheric current layer at height  $z_0$  above the surface of Earth and the flow of the electric current is toward the negative  $y$  axis (Figure 2). Let us denote this current in the spectral domain by

$$\tilde{j}_y(k_x, \omega) = \frac{1}{2\pi} \int_{-\infty}^{\infty} \int_{-\infty}^{\infty} j(x, t) e^{-i(k_x x + \omega t)} dx dt \quad (5)$$

where  $k_x$  is the wave number of the spatial fluctuations and  $\omega$  is the angular frequency of the temporal fluctuations. Now, immediately under the current sheet, the magnetic field can be expressed as [see, e.g., *Untiedt and Baumjohann, 1993*]

$$\tilde{B}_x^e(k_x, \omega, z_0) = \mu_0 \tilde{j}_y(k_x, \omega) / 2 \quad (6)$$

where  $\mu_0$  is the vacuum permeability and  $e$  denotes the external part of the magnetic field. As shown in Appendix A, the power spectrum of the magnetic field at the ionospheric level,  $|\tilde{B}_x^e(k_x, \omega, z_0)|^2$ , can be continued through the source free region ( $\nabla \times \mathbf{B} = 0$ ) to the surface of Earth ( $z = 0$ ) by computing

$$|\tilde{B}_x^e(k_x, \omega, 0)|^2 = |\tilde{B}_x^e(k_x, \omega, z_0)|^2 e^{-2z_0|k_x|} \quad (7)$$

Thus the continuation of the field away from the source is essentially low-pass filtering of the original field spectra. We emphasize that the field continuation does not explicitly affect the temporal scaling of the field spectrum (for additional discussion on this, see Appendix A). However, if  $k_x$  is a function of  $\omega$ , i.e., the spatial and temporal scalings are coupled, then temporal scaling is also affected by the field continuation. As a simple example of this kind of coupling consider a static magnetic field structure moving in the horizontal plane with a velocity  $v$  with respect to the observer. The relation between  $\omega$  and  $k_x$  is then simply  $\omega = vk_x$  and the field continuation affects the temporal scaling by a factor  $e^{-2z_0|k_x(\omega)|} = e^{-2z_0|\omega/v|}$ , i.e., the temporal field fluctuations are also low-pass filtered. As can be seen from the field continuation factor  $2z_0|k_x|$ , the effect on the temporal (and spatial) scalings is small if  $z_0 \ll |1/k_x|$ , i.e., for structures that have scale sizes much larger than the height of the ionosphere. However, without prior knowledge of the relation between  $k_x$  and  $\omega$ , it is impossible to estimate the effect on temporal scalings more in detail. Thus only the effects on the spatial scalings are treated in detail below.

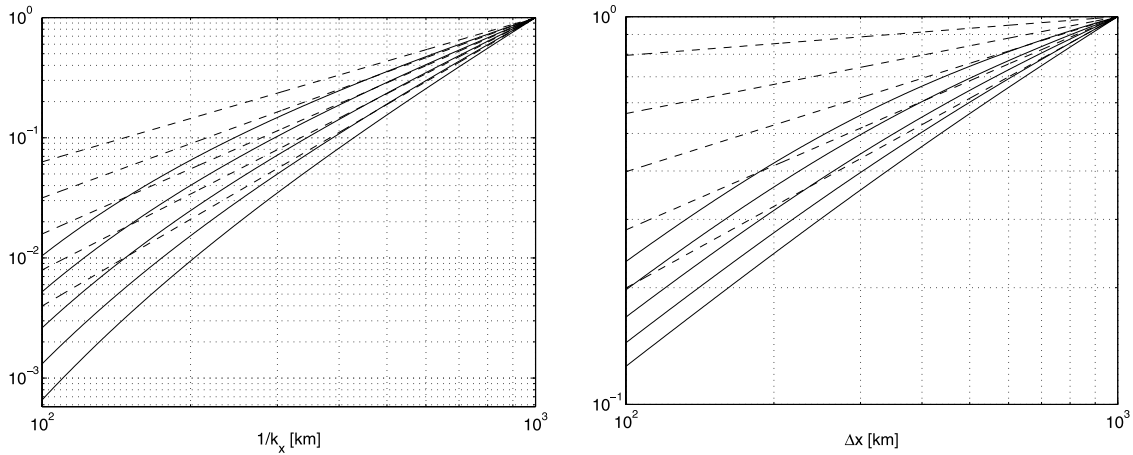


**Figure 3.** (left) Continued (solid lines) and original (dashed lines) external magnetic field spectra. (right) Structure function  $S^2(\Delta x)$  for continued (solid lines) and original (dashed lines) external magnetic field fluctuations. Original curves have power law scaling with exponent  $\beta$  equal to 1.2, 1.5, 1.8, 2.1, and 2.4 from top to the bottom.

[16] By using Fourier transforms of  $B_x^{e(x)}$  and  $B_x^e(x + \Delta x)$ , the structure function, as defined in equation (1), for the spatial magnetic field fluctuations can be expressed as

$$\begin{aligned} S^2(\Delta x) &= \langle |B_x^e(x) - B_x^e(x + \Delta x)|^2 \rangle \\ &= \frac{1}{2\pi} \int_{-\infty}^{\infty} \int_{-\infty}^{\infty} \langle \tilde{B}_x^e(k_x) \tilde{B}_x^e(k'_x)^* \rangle (e^{ik_x x} - e^{ik_x(x+\Delta x)}) \\ &\quad \cdot (e^{ik'_x x} - e^{ik'_x(x+\Delta x)})^* dk_x dk'_x \end{aligned} \quad (8)$$

where asterisk denotes a complex conjugate. Assuming that for the process under investigation it holds  $\langle \tilde{B}_x^e(k_x) \tilde{B}_x^e(k'_x)^* \rangle = \tilde{P}(k_x) \delta(k_x - k'_x)$  (for fully developed turbulence [e.g., Bohr et al., 1998, p. 19] and fractional Brownian motion [e.g., Hergarten, 2002, p. 49]  $\tilde{P}(k_x)$ , i.e., the power spectrum of the process obeys a power law), we obtain

$$S^2(\Delta x) = \frac{1}{\pi} \int_{-\infty}^{\infty} \tilde{P}(k_x) (1 - \cos(k_x \Delta x)) dk_x \quad (9)$$

Because the signal is real, the integrand in equation (9) is symmetric with respect to the origin and thus only positive wave numbers ( $k_x \geq 0$ ) need to be considered.

[17] Now, if the spatial scaling of  $|\tilde{j}_y(k_x, \omega)|^2$  and via equation (6) also that of  $|\tilde{B}_x^e(k_x, \omega, z_0)|^2$ , follows the power law spectrum, it follows from equation (7) that the scaling at the surface of Earth can be expressed as

$$|\tilde{B}_x^e(k_x, \omega, 0)|^2 = |\tilde{B}_x^e(k_x, \omega, z_0)|^2 e^{-2z_0 k_x} = c k_x^{-\beta} e^{-2z_0 |k_x|} \quad (10)$$

where  $c$  is a linear scaling constant and  $\beta$  is a spectral scaling exponent. In Figure 3 (left) the two spectra  $|\tilde{B}_x^e(k_x, \omega, 0)|^2$  and  $|\tilde{B}_x^e(k_x, \omega, z_0)|^2$  with  $z_0 = 100$  km are plotted for different  $\beta$ . As is clearly seen, significant distortions of the original scaling can be expected in

spatial scales between 100 and 1000 km. By substituting the right-hand side of equation (10) to equation (9) and by carrying out substitution  $u = k_x \Delta x$ , we obtain

$$S^2(\Delta x) = \frac{2c}{\pi} \Delta x^{\beta-1} \int_0^{\infty} u^{-\beta} e^{-\frac{2z_0 u}{\Delta x}} (1 - \cos(u)) du \quad (11)$$

For  $z_0 = 0$  equation (11) yields the familiar  $S^2(\Delta x) \sim \Delta x^{\beta-1}$  for  $1 < \beta < 3$ . For  $z_0 \neq 0$  one obtains

$$\begin{aligned} S^2(\Delta x) &= -\frac{2c}{\pi} 2^{\beta-1} \Gamma(1-\beta) z_0^{\beta-1} \left( \left( 1 + \frac{\Delta x^2}{4z_0^2} \right)^{\frac{1}{2}(\beta-1)} \right. \\ &\quad \cdot \left. \cos \left( (\beta-1) \tan^{-1} \left( \frac{\Delta x}{2z_0} \right) \right) - 1 \right) \end{aligned} \quad (12)$$

where the convergence at  $u = \infty$  requires that  $z_0/\Delta x \geq 0$  and the convergence at  $u = 0$  requires that  $\beta < 3$  and where  $\Gamma$  is the Gamma function. Note that in reality power laws do not extend from  $k_x$  (or  $u$ ) equals zero to  $\infty$  and thus the convergence requirements above are not absolute. In Figure 3 (right) are plotted the continued and original structure functions for different  $\beta$  with  $z_0 = 100$  km. As can be seen, the effect of the field continuation is surprisingly large especially for smaller  $\beta$ . The problem, for example, with the IMAGE magnetometer array data is that we are able to span scales only from about 100 to 1000 km, range which clearly is not reflecting directly the true power law scaling of the ionospheric currents if  $\beta$  is small.

[18] One should note that if the original scaling in the ionospheric level is not a power law, the results above do not necessarily hold. Consider, for example, original scaling of type

$$|\tilde{B}_x^e(k_x, \omega, z_0)|^2 = c e^{-2L|k_x|} \quad (13)$$

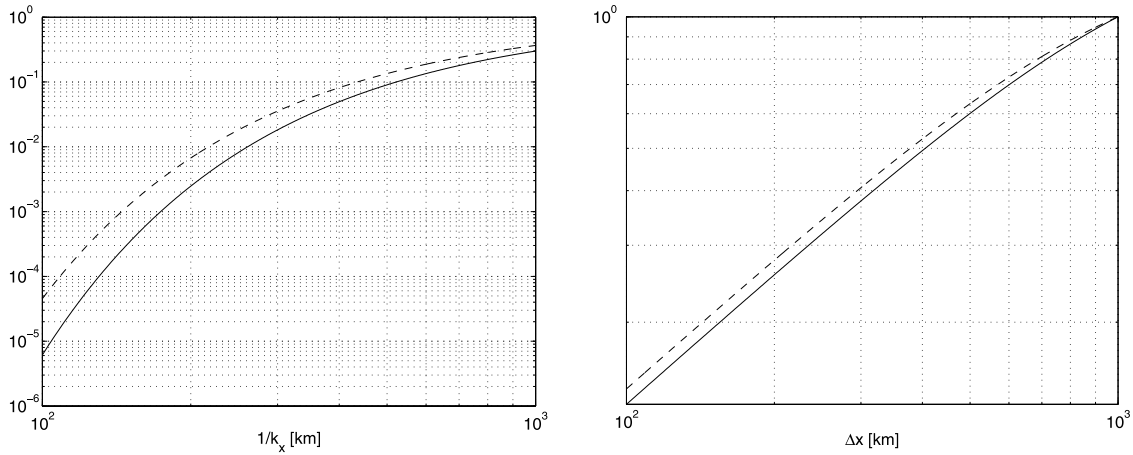


**Figure 4.** Same as in Figure 3 but for a function having an exponential spectral scaling. See the text for details.

where  $c$  and  $L$  are some positive constants. Now, by repeating the procedure above, one finds that the continued structure function reads

$$S^2(\Delta x) = \frac{c}{\pi} \frac{\Delta x^2}{4h^3 + h\Delta x^2} \quad (14)$$

where  $h = L + z_0$  and the convergence of the integral requires  $h/\Delta x \geq 0$ . From Figure 4, where the original and the continued functions with  $L = 500$  km and  $z_0 = 100$  km are again depicted, it is seen that in this case the continuation does not distort the scaling of the structure function severely. Thus it is clear that the effect of the field continuation is dependent on the original scaling; for power laws, containing abundant small-scale fluctuations the distorting effect is particularly severe.

[19] In fact, the exponential form of the spectrum in equation (13) is that of a current distribution

$$j(x, t) \sim \frac{I(t)}{L^2 + x^2} \quad (15)$$

where  $L$  is the half width of the current and  $I(t)$  describes the temporal behavior of the current amplitude. The current distribution in equation (15) can be used to describe the auroral electrojet [see, e.g., *Boteler et al.*, 2000] and accordingly, our choice  $L = 500$  km made above was not arbitrary but a realistic value to describe the spatial structure of the large-scale auroral electrojet.

[20] It should be noted that the results above hold also for the time derivative of the magnetic field. This can be seen formally by replacing  $B_x^e(x)$  by  $dB_x^e(x)/dt$  in equation (8) and by taking time derivative on both sides of equation (7) and by recalling that  $dB_x^e(k_x, \omega)/dt$  corresponds to  $i\omega B_x^e(k_x, \omega)$ . It is also worth noting that similar field continuation problem exist, in principle, in the interpretation of any magnetic field data. For example, spatial scaling analysis of the magnetospheric magnetic field measurements outside the source region faces identical scaling distortions to those described above.

[21] Summarizing, it was demonstrated that the field continuation may cause significant distortions to the origi-

nal ionospheric-level scalings. However, it was also shown that the amount of distortion is greatly dependent on the original scaling; for power law scalings the distortion is particularly severe. Without prior knowledge about the original ionospheric-level scaling, it obvious that field continuation causes additional ambiguity to the interpretation of the obtained results. Now, since we have no such prior information, the problem that we face also in trying to couple  $k_x$  and  $\omega$  (see above), it is inevitable that the interpretation of the spatial scalings will have the inherent uncertainty caused by the discussed effect. Unfortunately, the best we can do at this point is to acknowledge the existence of the ambiguity and go on with the analysis.

### 2.3. Effects of Geomagnetic Induction

[22] The magnetic field variations measured at the surface of Earth are composed of external and internal parts. The external part arises due to the sources in the ionosphere and magnetosphere, and the internal part is produced by currents induced within Earth by the temporally varying external source. Thus, before trying to interpret the external field characteristics from the scalings of the total measured magnetic field variations, one needs to know how the geomagnetic induction within Earth affects these scalings.

[23] The effects of the three-dimensional (3-D) induction in the determination of the ionospheric equivalent currents were investigated by *Pulkkinen and Engels* [2005] (herein-after referred to as PE04). In PE04, a 3-D ground conductivity model of the Fennoscandia was used to model the induction process excited by a realistic two-dimensional ionospheric equivalent source current. Model computations were carried out for a single substorm event of 26 June 1998. It was found that for temporal scales above about a few minutes, i.e., for frequencies below  $\sim 10$  mHz, the electromagnetic field penetrates to depths where 3-D distortions caused by the inhomogeneities at the surface layer do not cause significant spatial distortions to the determined ionospheric equivalent currents. Accordingly, it is reasonable to assume that the same holds true also for spatiotemporal statistics computed here. However, to minimize the 3-D effect, we exclude IMAGE stations that are experiencing some induction-related distortions due to their location in the

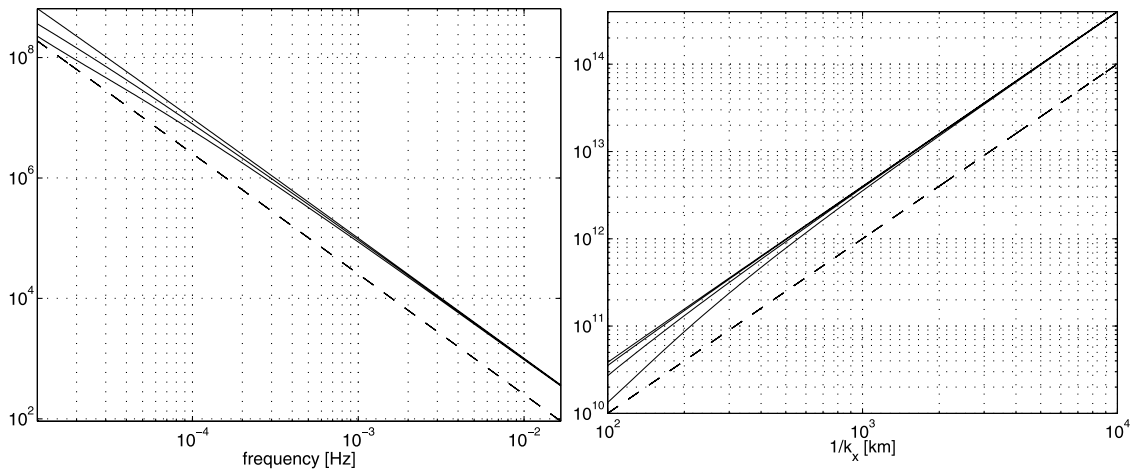


**Figure 5.** (left) Original, external magnetic field spectrum (dashed line) and the spectra distorted by the induction in 1-D Earth (solid lines) for different values of  $1/k_x$ . Values of  $1/k_x$  used are 100, 200, and 1000 km from the bottom to the top. (right) Original, external magnetic field spectrum (dashed line) and the spectra distorted by the induction in 1-D Earth (solid lines) for different periods  $1/f$ . Periods used are 60, 600, 6000, and 60,000 s from the top to the bottom. Original field fluctuations have power law exponent  $\beta$  equal to 2.

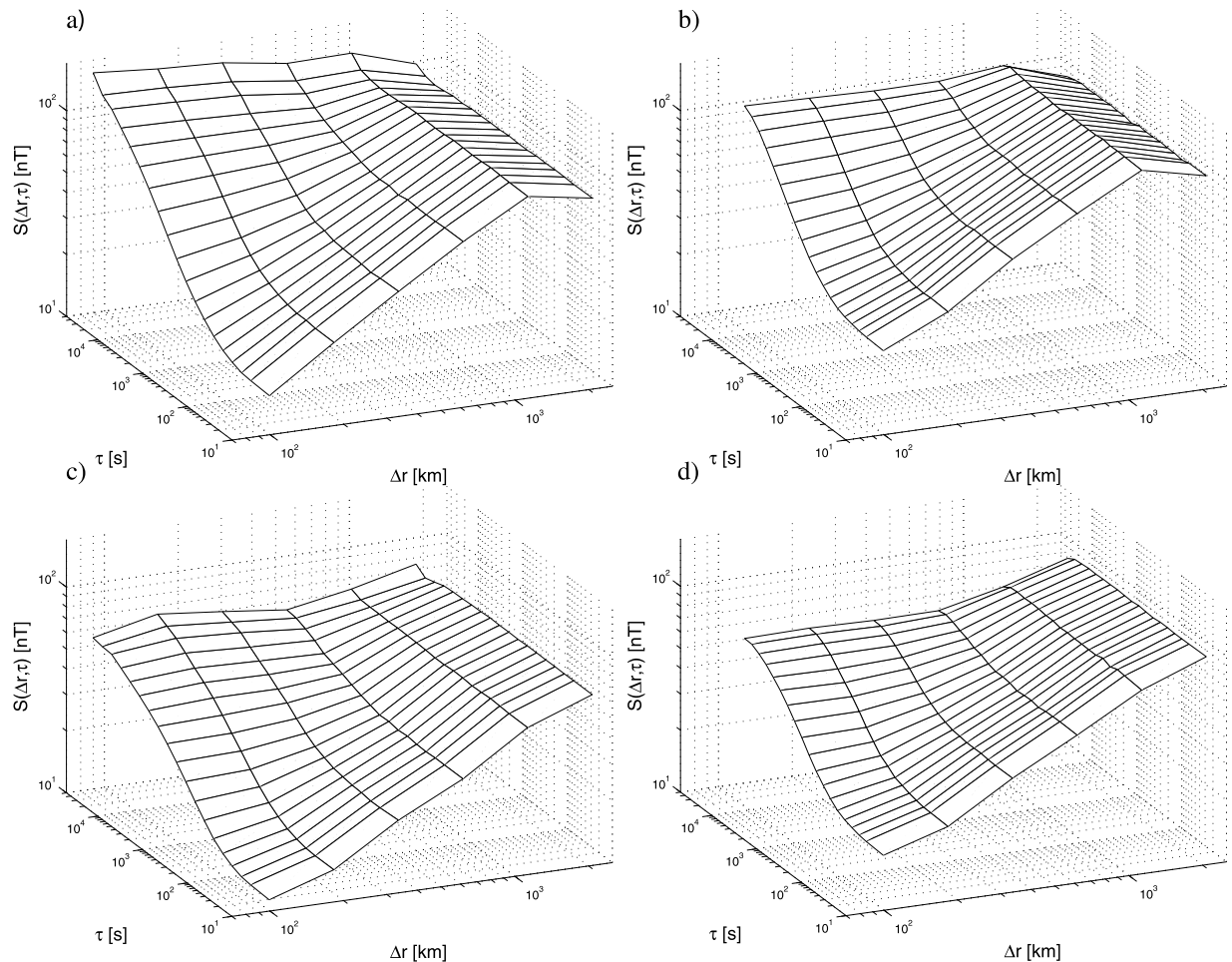


**Figure 6.** Spatiotemporal structure function  $S(\Delta r, \tau)$  of (a)  $B_x$  for the entire data set, (b)  $B_x$  for substorm events, (c)  $B_y$  for the entire data set, and (d)  $B_y$  for substorm events.

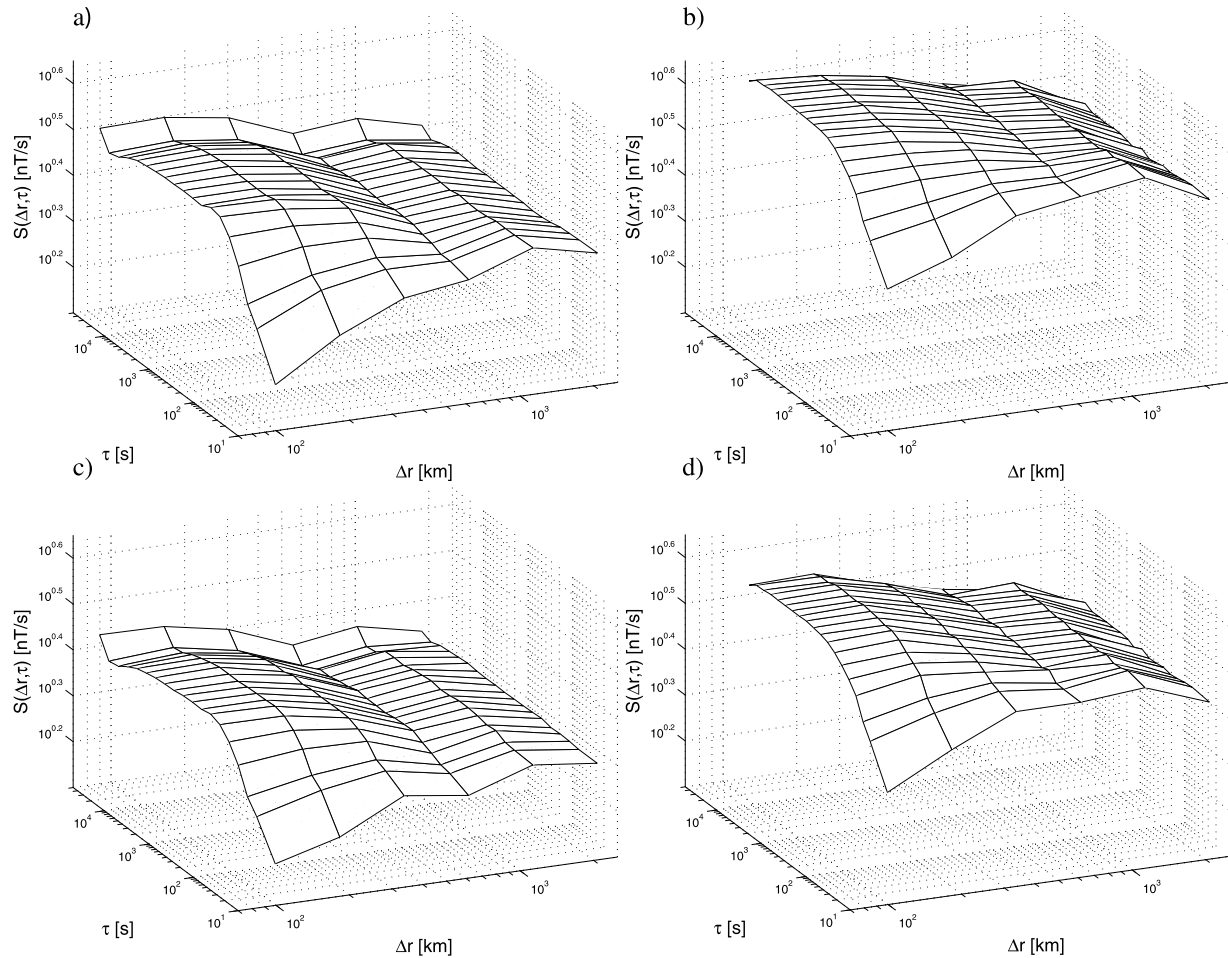


**Figure 7.** Spatiotemporal structure function  $S(\Delta r, \tau)$  of (a)  $dB_x/dt$  for the entire data set, (b)  $dB_x/dt$  for substorm events, (c)  $dB_y/dt$  for the entire data set, and (d)  $dB_y/dt$  for substorm events. Note the different scaling of the vertical axis to that in Figure 6.

vicinity of extreme conductivity gradients [see *Viljanen et al.*, 2001]. These stations were MAS, TRO, AND, and LYC (see Figure 1). Also LOZ was omitted due to some nongeophysical peculiarities in the data. Low-pass filtering suggested in PE04 was not carried out here because it would have introduced artificial cutoff effects in temporal scalings of the data.

[24] Despite the fact that 3-D effects of the surface inhomogeneities are probably relatively small, geomagnetic induction in the deeper, basically one-dimensional (1-D) structures of the Earth do affect the ionospheric currents determined from the total ground magnetic field data, as was found also in PE04. To investigate the effects of these 1-D structures, we use the 1-D ionospheric source current model used in section 2.2. Then, for 1-D Earth, the ratio between the internal and the external field components at the surface of Earth can be expressed as [see, e.g., *Berdichevsky and Zhdanov*, 1984, p. 193]

$$\frac{\tilde{B}_x^i(k_x, \omega, 0)}{\tilde{B}_x^e(k_x, \omega, 0)} = \frac{\frac{i\omega\mu_0}{k_x} + Z_s}{\frac{i\omega\mu_0}{k_x} - Z_s} = G \quad (16)$$

where  $Z_s$  is the spectral surface impedance and  $i$  denotes the internal part of the magnetic field. The surface impedance is

function of conductivities and thicknesses of layers in the 1-D Earth and can be evaluated using a simple recursive formula [see, e.g., *Berdichevsky and Zhdanov*, 1984, p. 54]. According to relation (16), the external part of the field is modified by induction as

$$\tilde{B}_x^{tot}(k_x, \omega, 0) = (1 + G)\tilde{B}_x^e(k_x, \omega, 0) \quad (17)$$

where *tot* denotes the total field measured at the surface of Earth. Note that  $G$  in equation (17) approaches unity as  $k_x$  approaches zero and thus it is clear that the spectral distortion caused by induction in 1-D Earth diminishes with increasing spatial scales; for planar source the distortion vanishes altogether.  $|\tilde{B}_x^{tot}(k_x, \omega)|^2$  for different values of  $k_x$  and  $\omega$  are plotted in Figure 5. The 1-D conductivity model of the central Finland [*Viljanen et al.*, 1999] was used in the computation of the spectral surface impedance.

[25] As seen from Figure 5, geomagnetic induction acts as a low-pass filter of spatial magnetic field fluctuations, and in contrast as a high-pass filter of temporal field fluctuations. For spatial scales above  $1/k_x = 100$  km and periods ( $1/f$ ,  $f$  frequency) below 6000 s, the spectral distortion caused by the induction is rather small. The most

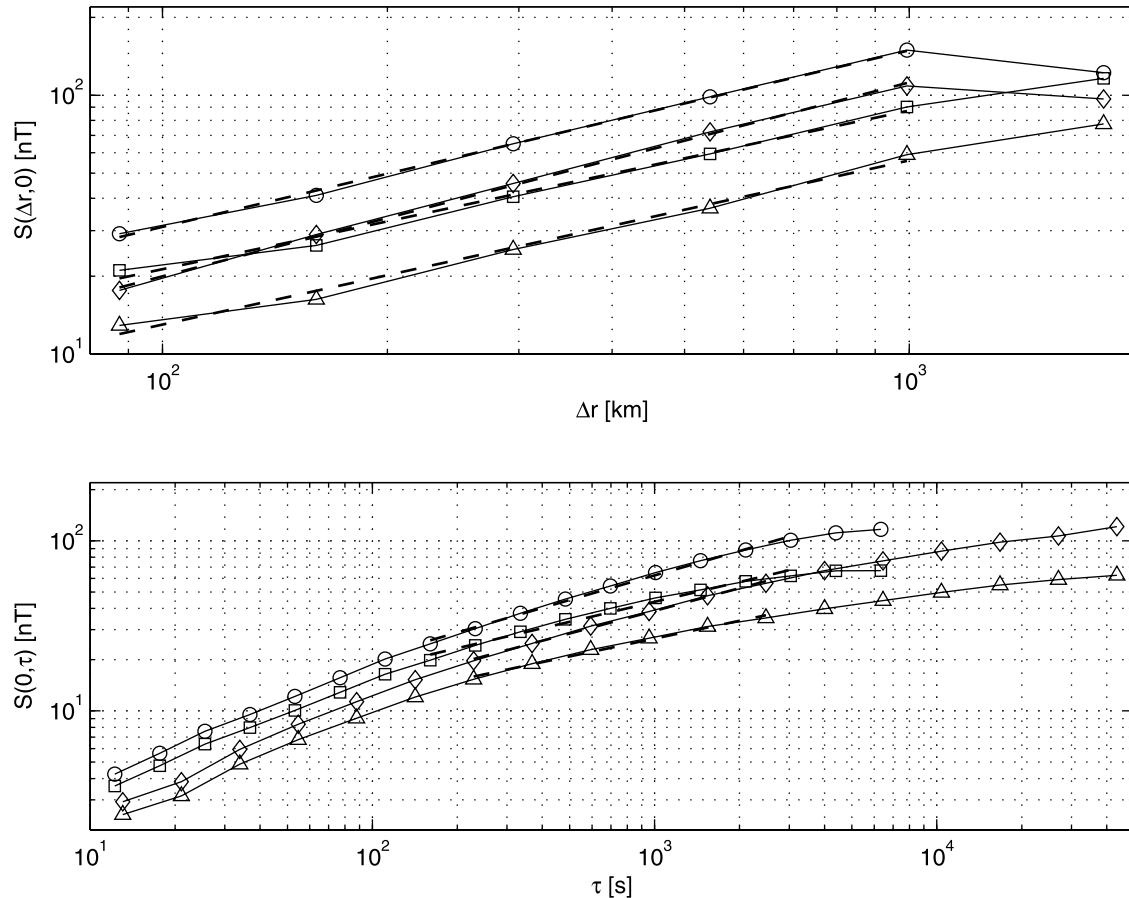


**Figure 8.** Structure functions (top)  $S(\Delta r, 0)$  and (bottom)  $S(0, \tau)$  and their least squares fits (dashed lines) for the magnetic field. Circles,  $S(\Delta r, 0)$  (Figure 8, top) and  $S(0, \tau)$  (Figure 8, bottom) for  $B_x$  of substorm events; diamonds,  $B_x$  of the entire data set; squares,  $B_y$  of substorm events; triangles,  $B_y$  of the entire data set. See Table 1 for the values of the fitted power law exponents. The fitted dashed curves are plotted for the range of values used in the fitting.

notable effect of the induction is the constant shift of the spectra to higher levels of spectral power: the scalings themselves are not much affected. Thus, although simple analytical mapping of the distorted Fourier spectra to the structure function cannot be made as in the case of the field continuation, we may conclude that for spatial scales larger than 100 km and temporal scales smaller than 6000 s induction does not significantly distort the original scalings of the external magnetic field fluctuations. However, the results presented here are strictly valid only for the particular Earth conductivity model used.

### 3. Scaling Properties

[26] Let us then turn to the actual measurements. Prior to analysis, visually detected daily baseline (quiet period) was removed from the 10 s resolution IMAGE array data. Then data were analyzed separately for each day of years 2002–2003 as described in section 2.1. The data set comprises the order of 100 million data points. After carrying out the daily analysis, the computed curves were averaged over different days to obtain the final scalings shown here.

[27] As was discussed above, the basic analysis contains statistics from a variety of different source currents in the

ionosphere and in the magnetosphere. To investigate separately the scalings of substorm time field fluctuations, we carried out the analysis also by using the substorm list compiled by *Tanskanen et al.* [2005]. In this case, the analysis was started from each onset of the substorm and was continued three hours forward in time for each event. Final substorm scalings were obtained by taking average over different events. Substorm events were taken from the years 2002–2003. The total number of analyzed substorm events was 499.

[28] Figures 6 and 7 show the full spatiotemporal structure functions  $S(\Delta r, \tau)$  for both  $x$  and  $y$  components of the field fluctuations and for both, the entire data set and the substorm events. Note that due to the logarithmic scale,  $S(\Delta r, 0)$  and  $S(0, \tau)$  are not shown. In Figures 8 and 9,  $S(\Delta r, 0)$  and  $S(0, \tau)$  of the full structure functions are shown with their power law fits. The power law exponents of the fits are given in Table 1. For clarity, in the following the properties of the magnetic field ( $B$ ) and the time derivative of the magnetic field ( $dB/dt$ ) fluctuations are described separately.

#### 3.1. Scaling Properties of $B$

[29] Comparisons to earlier studies can be made via Figure 8 (bottom) depicting  $S(0, \tau)$ . In a recent study by

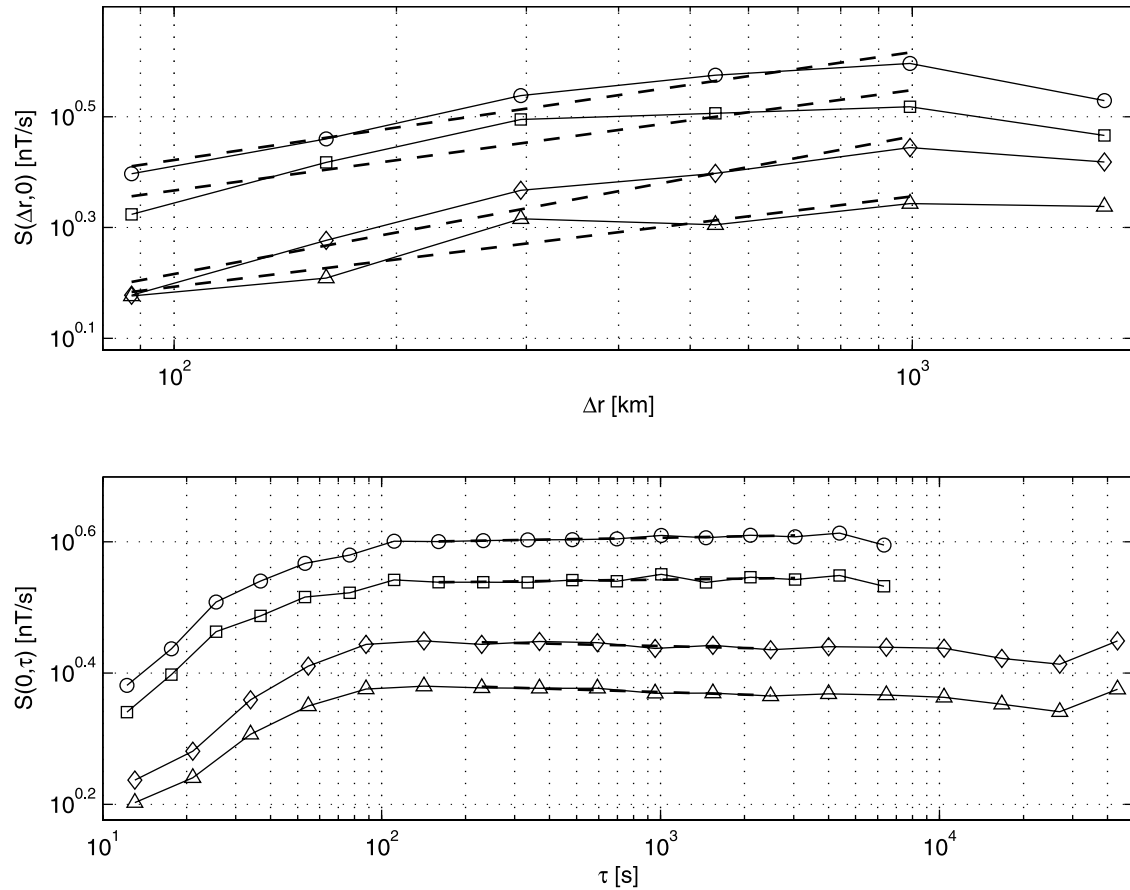


**Figure 9.** Structure functions (top)  $S(\Delta r, 0)$  and (bottom)  $S(0, \tau)$  and their least squares fits (dashed lines) for the time derivative of the magnetic field. Circles,  $S(\Delta r, 0)$  (Figure 9, top) and  $S(0, \tau)$  (Figure 9, bottom) for  $dB_x/dt$  of substorm events; diamonds,  $dB_x/dt$  of the entire data set; squares,  $dB_y/dt$  of substorm events; triangles,  $dB_y/dt$  of the entire data set. See Table 1 for the values of the fitted power law exponents. The fitted dashed curves are plotted for the range of values used in the fitting.

*Hnat et al.* [2002] the temporal scalings of  $AE$ ,  $AL$  and  $AU$  indices were investigated by studying the scaling of the indices via Relation (3). As was shown in section 2.1, theoretically, the scaling exponents  $H$  of *Hnat et al.* [2002] coincide with the scalings obtained from the structure function analysis carried out here. The power law exponent 0.44 obtained here for  $B_x$  fluctuations of the entire data set coincides well with exponents varying from 0.44 to 0.47 obtained for geomagnetic indices of *Hnat et al.* [2002] for the range of  $4 < \tau < 136$  min. However, no clear break in the scaling is observed at  $\tau$  equals 2 hours or 4 hours as in the scaling of geomagnetic indices [see also *Tsurutani et al.*, 1990; *Takalo et al.*, 1993]. This may result from averaging over different temporal scalings of different geomagnetic environments thus smearing the break or from the fact that

the data analyzed here is composed of, in contrast to auroral geomagnetic indices, continuous times series from single stations. If the absence of a clear break at the scales  $2 < \tau < 4$  hours is due to the latter reason, it is possible that the break seen in the time series of geomagnetic indices is at least partially an artifact due to the noncontinuous nature of the indices caused by the change of stations contributing to the signal. However, the appearance of the break in geomagnetic data from midlatitude stations analyzed by *Vörös et al.* [1998] and *Uritsky and Pudovkin* [1998] indicates that the absence of clear breaks in the scalings obtained here could be related to the former reason.

[30] Let us then focus on the aspects not seen in earlier investigations. A clear break is seen in Figure 6 where  $S(\Delta r, \tau)$  for  $B_x$  has a break essentially for all  $\tau$  at about  $\Delta r$  equals

**Table 1.** Power Law Exponents for fitted Curves in Figures 8 and 9<sup>a</sup>

	$S(\Delta r, 0), B$	$S(0, \tau), B$	$S(\Delta r, 0), dB/dt$	$S(0, \tau), dB/dt$
y component	$0.63 \pm 0.04$	$0.35 \pm 0.02$	$0.16 \pm 0.04$	$-0.01 \pm 0.002$
y component subs.	$0.61 \pm 0.03$	$0.39 \pm 0.02$	$0.18 \pm 0.04$	$0.01 \pm 0.003$
x component	$0.75 \pm 0.01$	$0.44 \pm 0.01$	$0.25 \pm 0.03$	$-0.01 \pm 0.004$
x component subs.	$0.68 \pm 0.02$	$0.48 \pm 0.01$	$0.19 \pm 0.03$	$0.01 \pm 0.001$

<sup>a</sup>Abbreviation subs. refers to substorms. See the text for details.

1000 km. The fact that this break is not seen as clearly in  $B_y$ , indicates that the break is related to the average size of the auroral electrojets affecting mainly  $B_x$  fluctuations. Below the break, roughly between  $100 < \Delta r < 1000$  km, a surprisingly good power law behavior of the spatial scaling  $S(\Delta r, 0)$  of  $B_y$ , and especially for  $B_x$  of the entire data set is observed. Keeping in mind that the effect of the magnetic field continuation distorts significantly the original ionospheric-level power law, it is likely that the initial spatial spectra of the ionospheric equivalent currents between  $100 < \Delta r < 1000$  km need not obey a power law. As was seen in Figure 4, other types of ionospheric-level scalings are also able to produce power-law-like scalings of the structure function between  $100 < \Delta r < 1000$  km.

[31] The overall spatiotemporal structure of the field fluctuations is relatively symmetric in terms of differences between  $x$  and  $y$  components seen in Figure 6 (the structure of the surfaces is very similar). Perhaps the most notable difference is the steeper break at  $\Delta r = 1000$  km in  $B_x$ , as was discussed above. In addition, as can be verified from Table 1, the exponents of the  $x$  component field fluctuations are systematically larger than those of  $y$  components. Also, as can be verified from Table 1 and Figure 6, the differences in the spatial structure of field fluctuations become smaller (the structure of the surfaces in Figure 6 becomes even more similar) during substorm events indicating increasing rotational symmetry of the fluctuations in the  $xy$  plane.

### 3.2. Scaling Properties of $dB/dt$

[32] Though no clear break was observed in the scaling of  $S(0, \tau)$  of  $B_x$  or  $B_y$ , at about  $2 < \tau < 4$  hours, a clear break in  $dB/dt$  occurs between  $80 < \tau < 100$  s. As can be observed from Figure 9 (bottom), between  $80 < \tau < 100$  s temporal fluctuations of  $dB/dt$  undergo a transition from a correlated signal to uncorrelated noise as expressed by very small (essentially zero) power law exponents. Interestingly, the spatial scaling (Figure 9, top) is indicative, keeping the ambiguity present in the interpretation of the spatial scalings discussed above in mind, of ionospheric-level power law scaling between  $100 < \Delta r < 1000$  km. Again the smoothest behavior is seen in the scaling of  $dB_x/dt$  of the entire data set. The obtained scaling exponent 0.25 coincides with ionospheric-level scaling exponent of 0.01 when fitted in least squares sense to equation (12). The other curves Figure 9 (top) yield values below 0.01 when fitted identically. This is indicating poor spatial correlations at zero time lag ( $\tau = 0$ ). With nonzero time lags we see evolution of  $S(\Delta r, \tau)$  (Figure 7): as a function of  $\tau$  we see transition of the  $\Delta r$  slope at about lag of 100 s from positive to negative. It is notable that the change in the spatial scalings coincide with the disappearance of the temporal correlations between  $80 < \tau < 100$  s. Thus, in terms of the time derivative of the ground magnetic field variations, dynamics of the spatio-temporal field fluctuations undergo a significant change at the scales between  $80 < \tau < 100$  s.

[33] As in the case of the  $B$  fluctuations, the overall spatiotemporal structure of the field fluctuations is relatively symmetric in terms of differences between  $x$  and  $y$  components seen in Figure 7. Also, as again can be verified from Table 1 and Figure 7, the differences in the spatial structure of field fluctuations become smaller during substorm

events. In addition to increasing rotational symmetry, another notable difference between field fluctuations of the entire data set and substorm time field fluctuations is the dip in the spatial structure of  $dB_x/dt$  and  $dB_y/dt$  at about  $\Delta r = 500$  km in  $S(\Delta r, \tau)$  of the entire data set that disappears for substorm events. This interesting feature is yet another indication of increasing spatial symmetry of substorm time field fluctuations.

### 4. Validity of the Magnetotelluric Relation

[34] In investigations based on the magnetotelluric sounding method [Cagniard, 1953], the planarity of the horizontal magnetic field variations has been a critical assumption on which the method heavily relies. The planarity condition is violated especially in auroral regions where the vicinity of a geometrically complex source causes nonuniform horizontal magnetic field variations [e.g., Mareschal, 1986]. However, recent magnetotelluric investigations in Fennoscandia have indicated that the method applied with robust processing using averaging of the electric field and magnetic field spectra over a number of different time intervals can be used to give stable estimates of the surface impedance up to periods of the order of 10,000 s even in the auroral region. The reason for this observation has remained unclear. We explore here, to what extent the observation can be explained by the scaling properties of the spatial magnetic field variations.

[35] Following Wait [1982, p. 187], we first define, by using the binomial theorem and by identifying the wave number with the spatial derivative, the spectral surface impedance for a homogeneous Earth as a derivative operator:

$$Z_s = \frac{\sqrt{\pi}}{2} \eta \sum_{n=0}^{\infty} \frac{1}{n! (\frac{1}{2} - n)!} \frac{1}{\gamma^{2n}} (-1)^n \left( \frac{\partial}{\partial x} \right)^{2n} \quad (18)$$

where  $\eta = \gamma / (\sigma + i\varepsilon_0\omega)$  and  $\gamma^2 = i\mu_0\omega(\sigma + i\varepsilon_0\omega)$  and  $\mu_0$ ,  $\varepsilon_0$  and  $\sigma$  indicate the vacuum permeability, the vacuum permittivity and the conductivity, respectively. The average of the electric field spectrum taken over number of different time intervals can be expressed as

$$\langle \tilde{E}_y(x) \rangle = -\frac{Z_s}{\mu_0} \langle \tilde{B}_x(x) \rangle \quad (19)$$

where  $\langle \cdot \rangle$  denotes again the expectation value and tilde is used to stress that fields are given in the frequency domain. Next we assume that the average behavior of the horizontal magnetic field variations with respect to the origin (i.e., we write  $\Delta x = x$ ) follows the power law:

$$\langle \tilde{B}_x(x) \rangle = cx^\alpha \quad (20)$$

where  $c$  is some constant and we assume that the power law holds for  $|x| < x_{max}$ . Fields  $\tilde{B}_x(x)$  and  $\tilde{E}_y(x)$  are now understood as deviations from the average values at the origin. Note that the scaling properties of the horizontal magnetic field data were investigated originally as a function of  $\Delta r = \sqrt{\Delta x^2 + \Delta y^2}$  but it is reasonable to assume that similar scaling holds also as a function of single coordinate  $\Delta x$ .

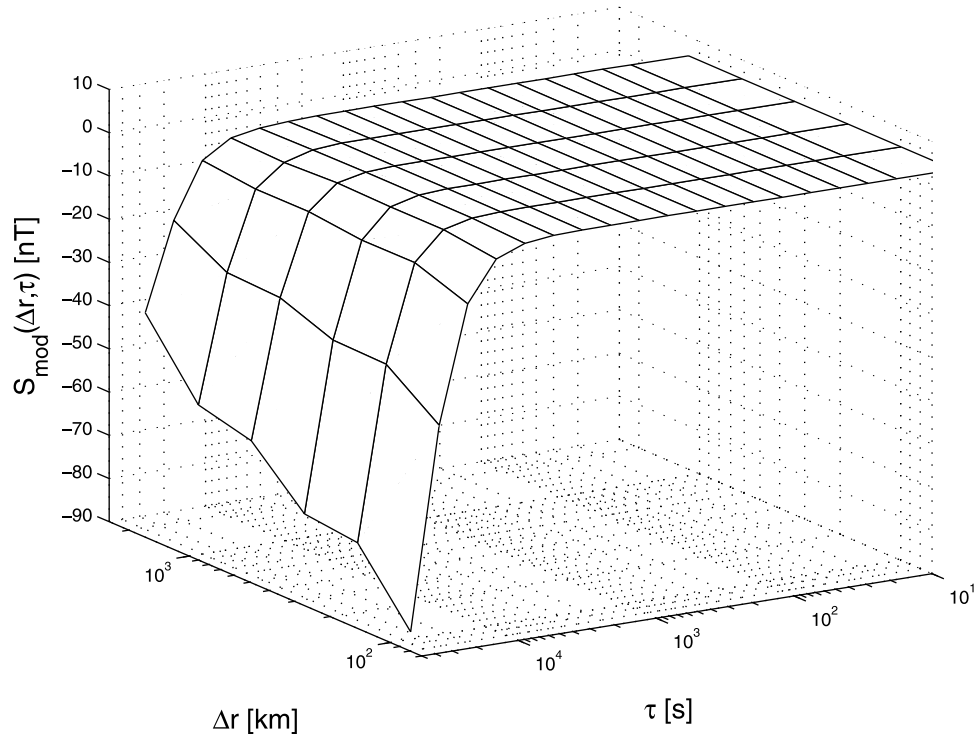


**Figure 10.**  $S_{mod}(\Delta r, \tau)$  of  $B_x$  for the entire data set. Note the linear scaling of the vertical axis.

[36] By inserting equations (18) and (20) into equation (19) we obtain

$$\langle \tilde{E}_y(x) \rangle = -\frac{\eta}{\mu_0} \langle \tilde{B}_x(x) \rangle - c \frac{\sqrt{\pi}}{2} \sum_{n=1}^{\infty} \frac{1}{n! (\frac{1}{2} - n)!} \frac{1}{\gamma^{2n}} (-1)^n \alpha^{2n} x^{\alpha - 2n} \quad (21)$$

where the first term on the right-hand side corresponds to the magnetotelluric relation and the second term we identify as  $G(\alpha, x, \gamma)$  expressing the deviation from this relation.

[37] Let us then investigate the convergence of  $G(\alpha, x, \gamma)$ . D'Alembert ratio test [see, e.g., *Arfken and Weber, 1995*, p. 290] gives us the following condition for the convergence of  $G(\alpha, x, \gamma)$ :

$$x^2 > \frac{\alpha^2}{|\gamma^2|} \quad (22)$$

where the right-hand side is the square of the radius of convergence  $R$ . So far we have not specified at which position  $x$  we want to evaluate equation (21). The natural choice is to carry out the evaluation at point  $x = x_{max}$ . Then, if  $R < x_{max}$ ,  $G(\alpha, x, \gamma)$  remains finite. For  $R \ll x_{max}$  convergence of  $G(\alpha, x, \gamma)$  is rapid and the magnetotelluric relation becomes a good approximation.

[38] Note that due to the derivative operator of equation (18), if  $\alpha$  is an positive integer, the sum in  $G(\alpha, x, \gamma)$  in equation (21) stops at  $\alpha-1$  for odd  $\alpha$  and at  $\alpha$  for even  $\alpha$  instead of  $\infty$ . Accordingly, for  $\alpha = 0$  or 1,  $G(\alpha, x, \gamma)$  vanishes. This well-known result means that if the spatial field variations vanish (plane wave) or are linear, the magnetotelluric relation holds exactly. For noninteger  $\alpha$

we need to investigate if the power law holds for distances larger than the radius of convergence  $R$  before stating anything about the validity of the magnetotelluric relation.

[39] The spatial magnetic field variations were investigated in previous sections as an absolute value of the difference in the field (equation (1)). However, the expression (19) (and accordingly equation (20)) does not contain absolute value of the field and thus the scaling results of section 3.1 cannot be used here. Thus we carried out additional computations in which the “modified structure function” was defined as

$$S_{mod}(\Delta r, \tau) = \langle a(t, \mathbf{r}) - a(t + \tau, \mathbf{r} + \Delta \mathbf{r}) \rangle \quad (23)$$

i.e., the analysis was repeated without taking the absolute value of the difference. The result of the repeated analysis of  $B_x$  for the entire data set is shown in Figure 10. As is easily seen,  $\alpha \approx 0$  for the spatial variations up to about  $\tau \approx 10,000$  s. This behavior of  $S_{mod}(\Delta r, \tau)$  provides a natural explanation of why the magnetotelluric relation holds in the auroral region up to periods of about 10,000 s: Below periods of 10,000 s the spatial variations of the horizontal magnetic field are symmetric causing a “flat,” or planar, average field and causing the magnetotelluric relation to hold exactly. Above periods of 10,000 s the symmetry in the field variations vanishes giving rise to a nonzero deviation  $G(\alpha, x, \gamma)$ .

[40] Quite interestingly, it is seen that magnetotelluric-sounding-related distortions are less severe in the auroral region than anticipated due to the symmetry of the spatial horizontal magnetic field variations that causes the average planar behavior. Obviously, the average planar behavior can

be obtained only if the averaging is carried out over a long enough time period. However, the convergence toward the scalings shown in Figure 10 is relatively rapid and essentially identical result is obtained already for 60 days of data (not shown here). In addition, we see that the requirement of planar or linear spatial behavior of the source field can possibly be relaxed to that of average power law type behavior as long as we can assume that the power law holds for spatial distances larger than the radius of convergence  $R$  for  $G(\alpha, x, \gamma)$ . The above discussion is, of course, valid only for homogeneous Earth and a more rigorous investigation is needed to put the suggestions given here on a firmer ground. However, based on the behavior of earlier theoretical generalizations in geomagnetic induction studies, like that of the complex image method [see *Wait and Spies, 1969; Thomson and Weaver, 1975*], it is certainly possible that the basic conclusions made above hold true also for a more general formulation of the problem.

## 5. Discussion

[41] Power law scalings of physical quantities are a fundamental property of modern theories used to describe the complexity in natural dynamic systems [see, e.g., *Sornette, 2004*]. To connect the observed fluctuations to a specific model, one needs a good confidence to fitted exponents of power laws that optimally describe the dynamics of the system over several orders of magnitude. Taking into account the effect of the field continuation causing inherent ambiguity to the interpretation of the obtained spatial scalings, it is all but clear how one should try to extract the nontrivial power law scalings of the magnetic field fluctuations from the spatiotemporal structure functions introduced here: poor power laws extending over less than an order of magnitude do not enable good confidence in the values of the fitted exponents. However, regardless of the existence of nontrivial power laws, the surfaces in Figures 6 and 7 contain an extensive amount of information about the dynamics driving the ground magnetic field fluctuations and any model constructed to reproduce the fluctuations should be able to capture at least some of the properties of these surfaces. Let us discuss these properties and their implications in the following.

[42] The most dramatic change in the observed dynamics occurred in the  $dB_x/dt$  and  $dB_y/dt$  fluctuations at temporal scales between  $80 < \tau < 100$  s. These scales are naturally linked to corresponding scales in the dynamics of the ionosphere-magnetosphere system. However, the link is all but self-evident and we postpone further speculations to forthcoming investigations. Above scales of 100 s, the temporal fluctuations of  $dB/dt$  had essentially trivial scaling, i.e., the scaling exponent was very close to zero; the same was true for spatial fluctuations of  $dB_x/dt$  and  $dB_y/dt$  for  $\tau = 0$  (when the effect of the field continuation was taken into account, i.e., for fluctuations at the ionospheric level). Thus, in a statistical sense, the spatiotemporal behavior of the time derivative of the horizontal ground magnetic variations at the ionospheric level, where the majority of the signal is presumably originating, is close to that of uncorrelated white noise. This has very important implications, for example, for the forecasts of ground effects of space weather which rely on correctly estimated temporal behav-

ior of the time derivative of the ground magnetic field. Uncorrelated white noise is completely unpredictable, and because of the close statistical resemblance between the white noise and  $dB_x/dt$  and  $dB_y/dt$  fluctuations, one is obligated to conclude the same about  $dB_x/dt$  and  $dB_y/dt$  fluctuations. This naturally implies that  $dB_x/dt$  and  $dB_y/dt$  fluctuations are not even in principle predictable in a deterministic way; nature sets boundaries for the accuracy with which we can forecast the future. These results are in line with the results by *Weigel and Baker [2003]* where the probability density function of  $dB_x/dt$  was observed to be invariant, for example, under different solar wind conditions. In another words,  $dB_x/dt$  are randomly drawn from a predefined distribution without direct correlation (possibly modifying the distribution) to driving conditions.

[43] Although  $dB_x/dt$  and  $dB_y/dt$  fluctuations are resembling statistically white noise, the amplitude of the noise is modulated by the general level of geomagnetic activity, i.e., larger amplitude fluctuations do occur during geomagnetically stormy conditions [*Viljanen et al., 2001*]. Thus, although the temporal behavior of the time derivative of the ground magnetic field may not be predictable in a deterministic sense, one can certainly say something about the likelihood of large amplitude fluctuations based on the level of overall geomagnetic activity.

[44] Another observed basic property of the magnetic field fluctuations is that the spatial symmetry clearly increases, i.e., the difference between the scaling behavior of the  $x$  and  $y$  components of the fluctuations decreases during substorm events. The preference for any particular direction or length scale decreases during substorms indicating the presence of poorly ordered equivalent current structures. By poorly ordered we mean that the probability for a current system to have a certain spatial orientation is decreased. This is an important extension to the classical view depicting the substorm current wedge as a current system flowing approximately in east-west direction [see, e.g., *Kamide and Kokobun, 1996*] which would imply difference between fluctuations in different magnetic field components. Fluctuations of the substorm time current systems are significantly less ordered in scales  $100 < \Delta r < 1000$  km than that of a simple east-west directed current flow. Quite interestingly, the increase (or restoration) of, for example, spatial symmetry of the fluctuations is a basic characteristic of turbulent system undergoing transition to a fully developed homogeneous turbulence [see, e.g., *Frisch, 1995*], indication that turbulence may play important role in the spatiotemporal evolution of the substorm time ionospheric equivalent currents. It should be noted that no division between expansion and recovery phases, having possibly different statistical characteristics, was made here.

## 6. Summary

[45] In this paper, the spatiotemporal scaling properties of the ground horizontal magnetic field fluctuations in the auroral region were investigated using of structure function analysis. We first studied the distorting effects of the continuation of the magnetic field from the ionosphere to the ground level and then the effects of the geomagnetic induction on the derived scalings. It was found that the

spatial fluctuations of the magnetic field and its time derivative are distorted by the field continuation in the ranges of scales of the data, i.e.,  $100 < \Delta r < 2400$  km and  $10 < \tau < 10^4$  s. Specifically, the extent of the distortion was found to be dependent on the original ionospheric-level scaling of the fluctuations; for power laws the distortion is particularly severe. The effect of the geomagnetic induction was found to be negligible in the ranges of scales of the data. It is noted that due to the spatial structure of the IMAGE magnetometer array, originally spatially two-dimensional analysis is rendered one-dimensional above scales of  $\sim 1000$  km.

[46] The main findings of the study are as follows. (1) There is significant change in the dynamics of the magnetic field fluctuations in the range  $80 < \tau < 100$  s where the time derivative of the magnetic field undergoes a transition from correlated to uncorrelated temporal behavior. (2) The spatiotemporal behavior of the time derivative of the magnetic field above temporal scales of 100 s resembles that of uncorrelated white noise; this may set constraints on the achievable forecasting accuracy of the time derivative of the magnetic field. (3) Spatial symmetry of the horizontal magnetic field fluctuations increases during substorms indicating the presence of spatially less ordered ionospheric equivalent currents. (4) The spatial scaling properties of the ground magnetic fluctuations may explain why the magnetotelluric sounding method works better than expected in auroral regions.

[47] In a follow-up of the present investigation we will explore why the good temporal power laws observed in the temporal fluctuations of geomagnetic indices were not repeated here. Breakdown of the analysis to single sites should reveal if this was due to varying temporal scaling, for example, as a function of latitude. We also intend to construct a more extensive statistical description of the field fluctuations in terms of probability density functions  $P(\Delta a, \tau)$  in the fashion of *Hnat et al.* [2002]. This type of a description may enable the construction of a dynamic model of field fluctuations. Yet another future work involves statistical joint analysis of auroral emissions (continuation of the work by *Uritsky et al.* [2002]) and ground magnetic field fluctuations. The main aim in this work is to move toward a more comprehensive stochastic description of the ionospheric electrodynamics.

## Appendix A: Derivation of the Field Continuation Factor

[48] Here we give a simple derivation of the factor in equation (7) used to carry out the continuation of the magnetic field away from the source in the ionosphere. Let us start from the standard telegraph equation for the magnetic field:

$$\nabla^2 \mathbf{B} = \mu_0 \sigma \frac{\partial \mathbf{B}}{\partial t} + \mu_0 \epsilon_0 \frac{\partial^2 \mathbf{B}}{\partial t^2} \quad (\text{A1})$$

where  $\mu_0$  and  $\epsilon_0$  are the vacuum permeability and permittivity, respectively and  $\sigma$  is the conductivity. Using a planar geometry which is reasonable for local studies like

the one carried out here, and the setting outlined in Figure 2, equation (1) transforms in the spectral domain for a nonconductive media (here air) into

$$\frac{\partial^2 \tilde{B}_x(k_x, \omega, z)}{\partial z^2} = \gamma^2 \tilde{B}_x(k_x, \omega, z) \quad (\text{A2})$$

where  $\gamma^2 = k_x^2 - \mu_0 \epsilon_0 \omega^2$  and  $k_x$  is the wave number of the spatial fluctuations and  $\omega$  is the angular frequency of the temporal fluctuations of the field. Since we are interested in the magnetic field that is continued away from the source, only the decaying solutions of equation (2) can be used and thus we have for the region below the source located at height  $z = -z_0$

$$\tilde{B}_x(k_x, \omega, z) = \tilde{B}_x(k_x, \omega, z_0) e^{-\gamma(z+z_0)} \quad (\text{A3})$$

At this point we note that  $\gamma$  is dependent both on the wave number and the frequency. However, for example for temporal fluctuations with period of 1 s, we have  $k_x^2 / \mu_0 \epsilon_0 \omega^2 \sim k_x^2 \cdot 10^{16}$  and thus the wave number term of  $\gamma$  is evidently dominating in the ranges of spatial and temporal scales that we are investigating. In another words, we can neglect the displacement current term of equation (1) and render the field continuation problem in a source-free media essentially into a static potential field problem. Accordingly, we obtain from equation (3) at  $z = 0$

$$|\tilde{B}_x(k_x, \omega, 0)|^2 = |\tilde{B}_x(k_x, \omega, z_0)|^2 e^{-2z_0|k_x|} \quad (\text{A4})$$

which is the expression we were looking for.

[49] **Acknowledgments.** The research was performed while A.P. and E.T. held National Research Council Associateship Awards at NASA/Goddard Space Flight Center. The work of A.P. and E.T. was supported also by the Academy of Finland. The IMAGE magnetometer array is an international project headed by the Finnish Meteorological Institute (<http://www.ava.fmi.fi/image/>). Fruitful discussions with A. Viljanen are greatly appreciated.

[50] Arthur Richmond thanks Simon Shepherd and another reviewer for their assistance in evaluating this paper.

## References

- Abel, G., and M. P. Freeman (2002), A statistical analysis of ionospheric velocity and magnetic field power spectra at the time of pulsed ionospheric flows, *J. Geophys. Res.*, *107*(A12), 1470, doi:10.1029/2002JA009402.
- Abel, G. A., M. P. Freeman, R. Nash, and G. Chisham (2004), A structure function analysis of ionospheric velocity and ground-based magnetic field fluctuations, *Eos Trans. American Geophysical Union*, *85*(47), Fall Meet. Suppl., Abstract NG23A-1191.
- Amm, O., and A. Viljanen (1999), Ionospheric disturbance magnetic field continuation from the ground to ionosphere using spherical elementary current systems, *Earth Planets Space*, *51*, 431–440.
- Arfken, G., and H. Weber (1995), *Mathematical Methods for Physicists*, 4th ed., Elsevier, New York.
- Barabási, A.-L., and H. E. Stanley (1995), *Fractal Concepts in Surface Growth*, Cambridge University Press.
- Berdichevsky, M., and M. Zhdanov (1984), *Advanced Theory of Deep Geomagnetic Sounding*, 408 pp., Elsevier, New York.
- Bohr, T., M. Jensen, G. Paladin, and A. Vulpiani (1998), *Dynamical Systems Approach to Turbulence*, Cambridge Univ. Press, New York.
- Borovsky, J. (2004), A model for the MHD turbulence in the Earth's plasma sheet: Building computer simulations, in *Multiscale Processes in the Earth's Magnetosphere: From Interball to Cluster*, pp. 217–254, Springer, New York.
- Boteler, D. H., R. Pirjola, and L. Trichtchenko (2000), On calculating the electric and magnetic fields produced in technological systems at the Earth's surface by a "wide" electrojet, *J. Atmos. Sol. Terr. Phys.*, *14*, 1311–1315.

- Buchert, S. C., R. Fujii, and K.-H. Glassmeier (1999), Ionospheric conductivity modulation in ULF pulsations, *J. Geophys. Res.*, *104*, 10,119–10,134.
- Burlaga, L. F. (1995), *Interplanetary Magnetohydrodynamics*, Oxford Univ. Press, New York.
- Cagniard, L. (1953), Basic theory of the magneto-telluric method of geophysical prospecting, *Geophysics*, *18*, 605–635.
- Chang, T., and S. Tam (2004), Complexity induced anisotropic bimodal intermittent turbulence in space plasmas, *Phys. Plasmas*, *11*, 1287–1299.
- Consolini, G., and P. De Michelis (2005), Local intermittency measure analysis of AE index: The directly driven and unloading component, *Geophys. Res. Lett.*, *32*, L05101, doi:10.1029/2004GL022063.
- Frisch, U. (1995), *Turbulence: The Legacy of A.N. Kolmogorov*, Cambridge Univ. Press, New York.
- Hergarten, A. (2002), *Self-organized criticality in Earth systems*, Springer, New York.
- Hnat, B., S. C. Chapman, G. Rowlands, N. W. Watkins, and M. P. Freeman (2002), Scaling of solar wind and the AU, AL and AE indices as seen by WIND, *Geophys. Res. Lett.*, *29*(22), 2078, doi:10.1029/2002GL016054.
- Kamide, Y., and S. Kokobun (1996), Two-component auroral electrojet: Importance for substorm studies, *J. Geophys. Res.*, *101*, 13,027–13,046.
- Klimas, A. J., V. M. Uritsky, D. Vassiliadis, and D. N. Baker (2004), Reconnection and scale-free avalanching in a driven current-sheet model, *J. Geophys. Res.*, *109*, A02218, doi:10.1029/2003JA010036.
- Kozelov, B. V., V. M. Uritsky, and A. J. Klimas (2004), Power law probability distributions of multiscale auroral dynamics from ground-based TV observations, *Geophys. Res. Lett.*, *31*, L20804, doi:10.1029/2004GL020962.
- Lui, A. T. Y., S. C. Chapman, K. Liou, P. T. Newell, C. I. Meng, M. Brittnacher, and G. K. Parks (2000), Is the dynamic magnetosphere an avalanching system?, *Geophys. Res. Lett.*, *27*, 911–914.
- Mareschal, M. (1986), Modelling of natural sources of magnetospheric origin in the interpretation of regional induction studies: A review, *Surv. Geophys.*, *8*, 261–300.
- Pulkkinen, A. (2003), Geomagnetic induction during highly disturbed space weather conditions: Studies of ground effects, *FMI Contrib.* *42*, Finn. Meteorol. Inst., Helsinki.
- Pulkkinen, A., and M. Engels (2005), The role of 3D geomagnetic induction in the determination of the ionospheric currents from the ground geomagnetic data, *Ann. Geophys.*, *23*, 909–917.
- Pulkkinen, A., O. Amm, A. Viljanen, and BEAR Working Group (2003), Separation of the geomagnetic variation field on the ground into external and internal parts using the spherical elementary current system method, *Earth Planets Space*, *55*, 117–129.
- Sornette, D. (2004), *Critical Phenomena in Natural Sciences: Chaos, Fractals, Self-Organization, and Disorder: Concepts and Tools*, 2nd ed., Springer, New York.
- Takalo, J., J. Timonen, and H. Koskinen (1993), Correlation dimension and affinity of AE data and bicolored noise, *Geophys. Res. Lett.*, *25*, 1527–1530.
- Tanskanen, E. I., J. A. Slavin, A. J. Tanskanen, A. Viljanen, T. I. Pulkkinen, H. E. J. Koskinen, A. Pulkkinen, and J. Eastwood (2005), Magnetospheric substorms are strongly modulated by high-speed streams, *Geophys. Res. Lett.*, *32*, L16104, doi:10.1029/2005GL023318.
- Thomson, D. J., and J. T. Weaver (1975), The complex image approximation for induction in a multilayered Earth, *J. Geophys. Res.*, *80*, 123–130.
- Tsurutani, B. T., M. Sugiura, T. Iyemori, B. E. Goldstein, W. D. Gonzalez, S. I. Akasofu, and E. J. Smith (1990), The nonlinear response of AE to the IMF B<sub>y</sub> driver: A spectral break at 5 hours, *Geophys. Res. Lett.*, *17*, 279–282.
- Untiedt, J., and W. Baumjohann (1993), Studies of polar current systems using the IMS Scandinavian magnetometer array, *Space Sci. Rev.*, *63*, 245–390.
- Uritsky, V. M., and M. I. Pudovkin (1998), Low frequency 1/f-like fluctuations of the AE-index as a possible manifestation of self-organized criticality in the magnetosphere, *Ann. Geophys.*, *16*, 1580–1588.
- Uritsky, V., A. Klimas, D. Vassiliadis, D. Chua, and G. Parks (2002), Scale-free statistics of spatiotemporal auroral emissions as depicted by POLAR UVI images: Dynamic magnetosphere is an avalanching system, *J. Geophys. Res.*, *107*(A12), 1426, doi:10.1029/2001JA000281.
- Viljanen, A., O. Amm, and R. Pirjola (1999), Modeling geomagnetically induced currents during different ionospheric situations, *J. Geophys. Res.*, *104*, 28,059–28,071.
- Viljanen, A., H. Nevanlinna, K. Pajunpää, and A. Pulkkinen (2001), Time derivative of the horizontal geomagnetic field as an activity indicator, *Ann. Geophys.*, *19*, 1107–1118.
- Viljanen, A., A. Pulkkinen, O. Amm, R. Pirjola, T. Korja, and BEAR Working Group (2004), Fast computation of the geoelectric field using the method of elementary current systems, *Ann. Geophys.*, *22*, 101–113.
- Vörös, Z., P. Kovács, Á. Juhász, A. Körmendi, and A. W. Green (1998), Scaling laws from geomagnetic time series, *Geophys. Res. Lett.*, *25*, 2621–2624.
- Wait, J. (1982), *Geo-electromagnetism*, Elsevier, New York.
- Wait, J., and K. Spies (1969), On the image representation of the quasi-static fields of a line current source above the ground, *Can. J. Phys.*, *47*, 2731–2733.
- Wanliss, J. (2005), Fractal properties of SYM-H during quiet and active times, *J. Geophys. Res.*, *110*, A03202, doi:10.1029/2004JA010544.
- Watkins, N. W., M. P. Freeman, S. C. Chapman, and R. O. Dendy (2001), Testing the SOC hypothesis for the magnetosphere, *J. Atmos. Sol. Terr. Phys.*, *63*, 1435–1445.
- Weigel, R. S., and D. N. Baker (2003), Probability distribution invariance of 1-minute auroral-zone geomagnetic field fluctuations, *Geophys. Res. Lett.*, *30*(23), 2193, doi:10.1029/2003GL018470.

A. Klimas, A. Pulkkinen, and D. Vassiliadis, NASA Goddard Space Flight Center, Code 612.2, Greenbelt, MD 20771, USA. (antti.pulkkinen@gsfc.nasa.gov)

V. Uritsky, Institute of Physics, St. Petersburg State University, St. Petersburg, 199034, Russia.

E. Tanskanen, Finnish Meteorological Institute, Space Research Unit, PO Box 503, FIN-00101 Helsinki, Finland.